Optimal control of non-Markovian dynamics in a single-mode cavity strongly coupled to an inhomogeneously broadened spin ensemble

Dmitry O. Krimer,[1,*] Benedikt Hartl,[1] Florian Mintert,[2] and Stefan Rotter[1]

[1]*Institute for Theoretical Physics, Vienna University of Technology (TU Wien), 1040 Vienna, Austria, EU*
[2]*Department of Physics, Imperial College, SW7 2AZ London, United Kingdom, EU*

Ensembles of quantum-mechanical spins offer a promising platform for quantum memories, but proper functionality requires accurate control of unavoidable system imperfections. We present an efficient control scheme for a spin ensemble strongly coupled to a single-mode cavity based on a set of Volterra equations relying solely on weak classical control pulses. The viability of our approach is demonstrated in terms of explicit storage and readout sequences that will serve as a starting point towards the realization of more demanding full quantum-mechanical optimal control schemes.

I. INTRODUCTION

In the past decade we have witnessed tremendous progress in the implementation of elementary operations for quantum information processing. Single-qubit gates can be realized with fidelities reaching $1-10^{-6}$ [1] and also two-qubit gates can be implemented in a variety of systems [2,3]. With all these elements at hand, it is nowadays possible to implement quantum algorithms on architectures with a few qubits (on the order of five) [4] and to engineer quantum metamaterials based on an ensemble of superconducting qubits coupled to a microwave cavity [5,6]. Implementing quantum logics on larger architectures, however, will most likely require a separation between quantum processing units and quantum memory units, where qubits in the former units admit fast gate operations and the qubits in the latter units offer long coherence times.

Since extended coherence times naturally imply weak interactions with other degrees of freedom, the sufficiently fast swapping of quantum information between processing and memory units is a challenging task. The most promising route to overcome slow swapping is the encoding of quantum information as a collective excitation in a large ensemble composed of many (N) constituents, since this increases the swapping speed by a factor of $\sqrt{N}$. Among promising realizations of such ensembles, those based on spins, atoms, ions, or molecules are of particular interest [7–13]. In many cases, however, system imperfections result in broadening effects giving rise to rapid dephasing of ensemble constituents, a restriction that limits the coherence times of such collective quantum memories.

As a result, various protocols to ensure the controlled and reversible temporal dynamics in the presence of inhomogeneous broadening were recently the subject of many studies. One of the proposed techniques in this context is the so-called controlled reversible inhomogeneous broadening approach [14–16], which is based on a rather subtle preparation method and on the inversion of atomic detunings during the temporal evolution. Most of the techniques developed for this purpose are based on photon-echo-type approaches in

cavity or cavityless setups, such as those dealing with spin refocusing [17,18], with atomic frequency combs [19–24], or with electromagnetically induced transparency [25]. Traditionally, these architectures operate in the optical region and require additional high-intensity control fields. The resulting large number of excitations is prone to spoil the delicate quantum information that is encoded in states with extremely low numbers of excitations. It would therefore be much better to work with low-intensity control fields, which, however, have the other problem to become easily correlated with the quantum memory. For the identification of control strategies, this implies that one may no longer treat the many different memory spins as independent objects, but that the (macroscopically) large ensemble needs to be described by a quantum many-body state. This makes any description of dynamics and an identification of control strategies a seemingly hopeless task.

In this paper we develop a very efficient semiclassical optimization technique based on a set of Volterra integral equations, which allows us to write information into a large, inhomogeneously broadened spin ensemble coupled to a single-cavity mode by means of optimized classical microwave pulses and to retrieve it at some later time in the form of well-separated cavity responses. In contrast to established echo techniques, our scheme only involves low-intensity signals and therefore diminishes the influence of noise caused by writing and reading pulses. The applicability of our approach is also demonstrated in conjunction with a spectral hole-burning technique [26–28] that allows us to reach storage times going far beyond the dephasing time of the inhomogeneous broadened ensemble. Importantly, the Volterra equation exactly governs the resulting linear non-Markovian dynamics not only in the semiclassical but also in the pure quantum case for the particular situation without external drive, when all spins are initially in the ground state and the cavity contains initially a single photon [26,28,29]. Furthermore, the system's density function or nonequilibirum Green's functions, which show up in the framework of a full quantum-mechanical description, also satisfy mathematically similar integro-differential Volterra equations [30,31]. Hence, although the problem is treated semiclassically in what follows, we believe that our approach can be generalized to pure quantum regimes as well in which case the inclusion of the

_____
*dmitry.krimer@gmail.com
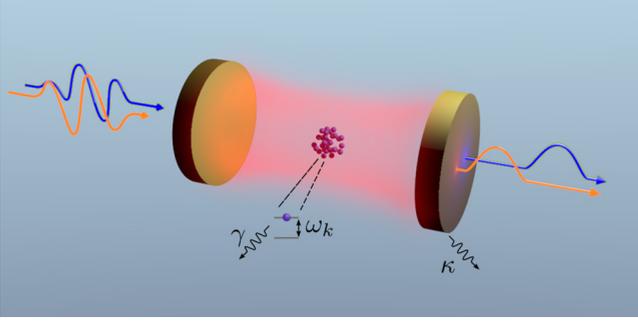
FIG. 1. Schematics of a single-mode cavity characterized by a frequency ω_c and a loss rate κ, coupled to an ensemble of two-level atoms (spheres) with transition frequencies ω_k and a loss rate $\gamma \ll \kappa$. Curves designate optimized input and (nonoverlapping) output signals.

transient two-time correlation function of the cavity operator between the write and the readout may be needed, an issue that will be postponed for future studies.

II. THEORETICAL MODEL

To be specific, we consider an ensemble of spins strongly coupled to a single-mode cavity via magnetic or electric dipole interaction as sketched in Fig. 1. All typical parameter values are chosen here in accordance with the recent experiment [29], the dynamics of which can be excellently described by the Tavis-Cummings Hamiltonian [32] (in units of $\hbar$)

$$\mathcal{H} = \omega_c a^\dagger a + \frac{1}{2} \sum_j^N \omega_j \sigma_j^z + i \sum_j^N [g_j \sigma_j^- a^\dagger - g_j^* \sigma_j^+ a]$$
$$- i[\eta(t) a^\dagger e^{-i\omega_p t} - \eta(t)^* a e^{i\omega_p t}]. \quad (1)$$

Here $\sigma_j^\pm$ and σ_j^z are the Pauli operators associated with each individual spin of frequency ω_j and $a^\dagger$ and a are creation and annihilation operators of the single cavity mode with frequency ω_c. An incoming signal is characterized by the carrier frequency ω_p and by the envelope $\eta(t)$. The interaction part of $\mathcal{H}$ is written in the dipole and rotating-wave approximation (terms proportional to $a\sigma_j^-$ and $a^\dagger\sigma_j^+$ are neglected), where g_j is the coupling strength of the jth spin. The distance between spins is assumed to be large enough such that the direct dipole-dipole interactions between spins can be neglected. Furthermore, the large number of spins allows us to enter the strong-coupling regime of cavity QED with the collective coupling strength $\Omega = (\sum_j^N g_j^2)^{1/2}$ [33], which leads to the enhancement of a single coupling strength g_j by a factor of $\sqrt{N}$ ($N \approx 10^{12}$ in [29]).

We are aiming at the transfer of information from the cavity to the spin ensemble, its storage over a well-defined period of time, and its transfer back to the cavity. Our control scheme thus consists of a write and readout section, with a variable delay section in between. Starting from a polarized state with all spins in their ground state, we construct (i) two write pulses $\eta_{|0\rangle}^{(W)}(t)$ and $\eta_{|1\rangle}^{(W)}(t)$ that encode the respective logical states $|0\rangle$ and $|1\rangle$ in the spin ensemble. During the delay section (ii) the information is subject to dephasing by the inhomogeneous ensemble broadening and the external drive is optimized here

to reduce the cavity amplitude $A(t) \equiv \langle a(t) \rangle$ (to prevent the information in the spin ensemble from leaking back to the cavity prematurely). In the readout section (iii) we switch on the readout pulse $\eta^{(R)}(t)$ [with substantially lower power than $\eta_{|0/1\rangle}^{(W)}(t)$] that maps the two logical states of the spin ensemble on two mutually orthogonal states of the cavity field, expressed by the cavity amplitude $A_{|0\rangle}^{(R)}(t)$ or $A_{|1\rangle}^{(R)}(t)$, respectively. Note that the write pulses (i) are specific for the input states $|0\rangle$ and $|1\rangle$, but pulses (ii) and (iii) are generic as they are designed without prior knowledge of the information stored in the ensemble. [For the sake of simplicity we formally absorb the delay pulse into $\eta^{(R)}(t)$.] The goal of our work is to find optimal time-dependent choices for $\eta_{|0\rangle}^{(W)}(t)$, $\eta_{|1\rangle}^{(W)}(t)$, and $\eta^{(R)}(t)$ such that $A_{|0\rangle}^{(R)}(t)$ and $A_{|1\rangle}^{(R)}(t)$ have minimal temporal overlap in analogy to time-binned qubits where information is stored in the occupation amplitudes of two well-distinguishable time bins [20,34].

We describe the dynamics by deriving the equations for the spin and cavity expectation values $\langle \sigma_k^-(t) \rangle$ and $A(t)$ under the Holstein-Primakoff-approximation [35] ($\langle \sigma_k^{(z)} \rangle \approx -1$) valid in the regime of weak driving powers (the number of the excited spins is always small compared to the ensemble size). This allows us to formally express $\langle \sigma_k^-(t) \rangle$ as a time integral with respect to $A(t)$ and to develop an efficient framework in terms of Volterra equations that relate cavity amplitudes $A(t)$ and pump profiles $\eta(t)$ [36],

$$A(t) = \int_0^t d\tau \, \mathcal{K}(t-\tau) A(\tau) + \mathcal{D}(t), \quad (2)$$

where $\mathcal{D}(t)$ depends on the time integral of the driving signal and on the initial conditions for the cavity amplitude as well as of the spin ensemble. The memory kernel function $\mathcal{K}(t-\tau)$, which is responsible for the non-Markovian feedback of the spin ensemble on the cavity, is proportional to the collective coupling strength Ω^2 and explicitly depends on a spectral spin distribution characterized by a function $\rho(\omega)$ (see Appendix A). When switching on a constant drive, the system exhibits damped oscillations characterized by the Rabi frequency $\Omega_R \approx 2\Omega$ and the total decoherence rate Γ mostly determined by the dephasing caused by the inhomogeneous broadening of the spin ensemble [36].

A consequence of the linearity of the governing Volterra equations is that for two pump profiles $\eta_{1/2}(t)$, resulting in the two cavity amplitudes $A_{1/2}(t)$, any coherent superposition of these pulses $c_1\eta_1(t) + c_2\eta_2(t)$ will result in the corresponding cavity amplitudes $c_1 A_1(t) + c_2 A_2(t)$.

The Volterra equation for the cavity amplitude is physically the classical correspondence of the Heisenberg cavity spin equations on the level of expectation averages after elimination of the spin ensemble variables (see Appendix A). However, as was demonstrated in [26,29,37], the Volterra equation also governs quantum spin–cavity dynamics for the particular case when all spins are initially in the ground state and the cavity contains initially a single photon. Therefore, we take the amplitude of the write pulses $\eta_{|0/1\rangle}^{(W)}(t)$ such that the net power injected into the cavity corresponds to the power of a coherent driving signal with an amplitude equal to the cavity decay rate κ. The latter prepares on average a single photon in the empty cavity for stationary transmission experiments (see

Appendix D for details). Due to the linearity of the Volterra equations, also rescaling their solutions by a global prefactor leaves them perfectly valid.

III. OPTIMAL CONTROL SCHEME

As a first step we need to find optimal write and readout pulses that prepare the logical spin ensemble configurations $|0\rangle$ and $|1\rangle$ and map them onto well-distinguishable cavity responses. We do this through the optimization of a functional, which ensures the minimal overlap between the cavity amplitudes $A_{|0\rangle}^{(R)}(t)$ and $A_{|1\rangle}^{(R)}(t)$ of the logical states $|0\rangle$ and $|1\rangle$ in the readout section by exploring various temporal shapes of both the write pulses $\eta_{|0/1\rangle}^{(W)}(t)$ and of the readout pulse $\eta^{(R)}(t)$. In practice we expand all involved driving pulses in a basis of trial functions $\sin(n\omega_f t)$ ($n = 1, 2, \ldots$) with the fundamental frequency ω_f defined as the inverse of the time duration of the write or readout section counted in multiples of half the Rabi period π/Ω_R. Next we construct the functional defined as the time-overlap integral between $A_{|0\rangle}^{(R)}(t)$ and $A_{|1\rangle}^{(R)}(t)$ in the readout section. We then search the functional's minima under several constraints considering the expansion coefficients as unknown variables using the standard method of Lagrange multipliers (see Appendixes A and B). Due to the linearity of governing equations with respect to the control pulses this procedure, as shown in Appendix B, is numerically highly efficient since the time integration of the Volterra equations can be performed independently of the subsequent optimization of the expansion coefficients of the control pulses.

A typical result of this optimization (first without a delay section) is depicted in Fig. 2 (left column), where the amplitudes of all optimized pulses as well as those of the resulting cavity responses are depicted. One can indeed see that the two different configurations stored in the spin ensemble, $|0\rangle$ and $|1\rangle$, are retrieved by the same readout pulse in the form of two well-separated cavity responses. The storage efficiency can be quantified in terms of the ratio of integrated cavity amplitudes during the readout and write section, which turns out to be $\approx 40\%$ for the configurations $|0\rangle$ and $|1\rangle$ shown in Fig. 2 (left column).

The bottleneck for extended information storage times in the ensemble is its inhomogeneous broadening, as determined by the continuous spectral density $\rho(\omega)$ appearing in our theoretical description. Specifically, the total decoherence rate in the limit of strong coupling (when $\Omega > \Gamma$) can be estimated as $\Gamma \approx \kappa + \pi\Omega^2\rho(\omega_s \pm \Omega)$ [36,37], indicating that the dominant contribution to Γ stems from the spectral density $\rho(\omega)$ at frequencies close to the maxima of the two polaritonic peaks $\omega = \omega_s \pm \Omega$. To suppress this decoherence rate Γ it is thus advisable to work with spin ensembles having a spectral density that falls off faster than $1/\Omega^2$ in its tails such that $\Gamma \to \kappa$ for large Ω. The corresponding cavity protection effect [36–38] has meanwhile been demonstrated also experimentally [29], but has the drawback of requiring prohibitively large coupling strengths to take full effect. Alternatively, one can burn two narrow spectral holes at frequencies close to $\omega_s \pm \Omega$, during a preparatory step for $t \leqslant 0$. This technique [26–28] was recently shown to be both easily implementable and very efficient in suppressing the decoherence rate Γ even below the bare cavity decay

rate κ [27]. Incorporating this hole-burning protocol in the present analysis allows us to increase the dephasing time from $1/\Gamma \sim 75$ ns [the case shown in Fig. 2 (left column)] to microsecond time scales [see Fig. 2 (right column)] for which we can now meaningfully introduce a delay section in between the write and the readout section. In Fig. 2 (right column) we show that with parameters taken from recent experiments [27] we can extend the storage time and thereby our method's temporal range of control beyond 1 μs. Evidently, such an extension of the storage time comes with a reduced efficiency, which is here as large as 5%.

With these long coherence times we can now proceed to the main goal of storing coherent superpositions of the two spin configurations $|0/1\rangle$. Those can be created by the corresponding superposition $\eta^{(W)}(t) = \alpha\eta_{|0\rangle}^{(W)}(t) + \beta\eta_{|1\rangle}^{(W)}(t)$ of the respective write pulses and, ideally, the corresponding superposition of time-binned cavity responses would be observed under the application of the readout pulse $\eta^{(R)}(t)$. Since the cavity response is of the form $A^{(R)}(t; \alpha, \beta) = \alpha\tilde{A}_{|0\rangle}^{(R)}(t) + \beta\tilde{A}_{|1\rangle}^{(R)}(t) + \tilde{A}^{(R)}(t)$, where the two cavity responses $\tilde{A}_{|0/1\rangle}^{(R)}(t)$ only depend on the stored spin configurations $|0/1\rangle$ and $\tilde{A}^{(R)}(t)$ is the response induced by the readout pulse, the desired superposition of cavity outputs is obtained if the readout pulse satisfies $(\alpha + \beta)\eta^{(R)}(t) = \eta^{(R)}(t)$ (see Appendix B). Together with the normalization $|\alpha|^2 + |\beta|^2 = 1$, this implies that for the amplitudes $\alpha_x = 1 - x \pm i\sqrt{x(1-x)}$ and $\beta_x = x \mp i\sqrt{x(1-x)}$ with $x \in [0, 1]$ the desired cavity response will be obtained. As a result, the proposed storage sequence works not only for the two logical basis states $|0/1\rangle$, but, indeed, for a one-dimensional set of coherent superpositions, such as for a rebit [34,39].

Note that when being only interested in reading out the parameters α and β (and not in further processing the resulting cavity response) one is not restricted by the above rebit parametrization, but has the full qubit parameter space at one's disposal. As we show in Appendix B, α and β can be unambiguously determined through the time-overlap integrals defined only in the readout section $[\tau_a, \tau_c]$ as $\mathcal{O}_{0/1} = \int_{\tau_a}^{\tau_c} dt\, A^{(R)}(t; \alpha, \beta)A_{|0/1\rangle}^{(R)*}(t)$, where $A_{|0/1\rangle}^{(R)}(t) = \tilde{A}_{|0/1\rangle}^{(R)}(t) + \tilde{A}^{(R)}(t)$.

In principle, this information retrieval is exact, but noise (which is not included in the previous theoretical modeling) affects the readout if it reaches values comparable to the cavity amplitudes. Therefore, in the next line of our study we examine the robustness of our optimal control scheme against possible noise. For that purpose, we subject the previously established optimized pulses $\eta_{|0/1\rangle}^{(W)}(t)$ and $\eta^{(R)}(t)$ to a small perturbation by adding Gaussian white noise as an additional driving term in our Volterra equations (see Appendix C). We treat the problem numerically using well-established methods for integrating stochastic differential equations (see, e.g., [40]) and accumulate statistics by evaluating many trajectories for different noise realizations. We then average the resulting retrieved values with respect to noise realizations and calculate the absolute retrieval errors as the deviation from the input configuration, $\epsilon_\alpha = |\alpha - \langle\alpha_\mathcal{R}\rangle|$ and $\epsilon_\beta = |\beta - \langle\beta_\mathcal{R}\rangle|$. The typical results of our calculations are displayed in Fig. 3. It turns out that ϵ_α and ϵ_β scale approximately linearly with the noise amplitude and, e.g., the maximal absolute error
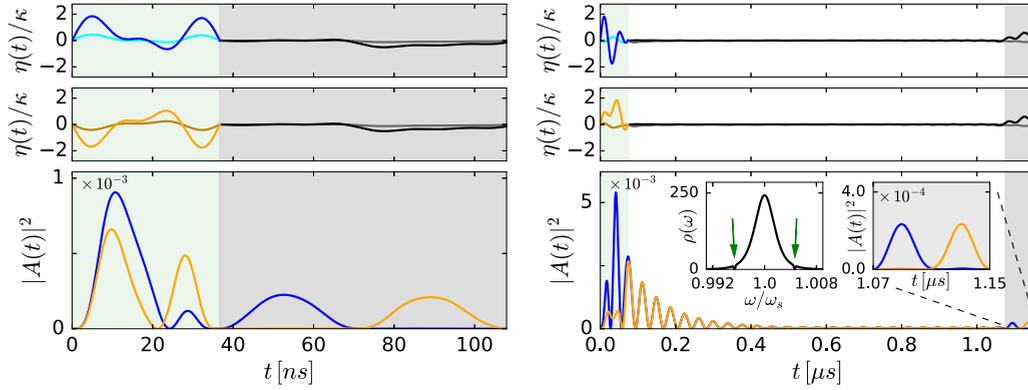
FIG. 2. Preparation of the spin ensemble configurations $|0\rangle$ and $|1\rangle$ for a spin density $\rho(\omega) = C[1 - (1 - q)(\omega - \omega_s)^2/\Delta^2]^{1/(1-q)}$ following a q-Gaussian distribution with $q = 1.39$ centered around the cavity frequency $\omega_s = \omega_c$ and a full width at half maximum $\gamma_q = 2\Delta\sqrt{(2^q - 2)/(2q - 2)} = 2\pi \times 9.4$ MHz. This form for $\rho(\omega)$ was established in our previous studies by a careful comparison with the experiment [29,36]. The right column shows that two holes were burnt into $\rho(\omega)$ at frequencies $\omega_s \pm \Omega$ (two arrows in the inset) to suppress decoherence [26,27] and to make room for a delay section (white area) between the write [green area (light gray)] and readout (gray area) sections. [In the inset $\rho(\omega)$ is plotted in units of ω_s^{-1}.] The top and middle rows show real [blue (dark gray) and orange (light gray), respectively] and imaginary parts [cyan (light gray) and brown (dark gray), respectively] of the optimized write pulse $\eta_{|0/1\rangle}^{(W)}(t)$ for state $|0/1\rangle$ and of the generic readout pulse $\eta^{(R)}(t)$ (black and gray). The bottom row shows the cavity probability amplitude squared $|A(t)|^2$ for the resulting nonoverlapping cavity responses $A_{|0\rangle}^{(R)}(t)$ [blue (dark gray)] and $A_{|1\rangle}^{(R)}(t)$ [orange (light gray)]. The carrier frequency of all pulses $\omega_p = \omega_c = 2\pi \times 2.6915$ GHz and the coupling strength $\Omega/2\pi = 12.5$ MHz. The ratio of the powers between the readout and write pulses is 0.068 (0.013) for the case without (with) hole burning. The amplitudes of all pulses (top and middle rows) are presented in units of $\kappa/2\pi = 0.4$ MHz.

of retrieval shown in Fig. 3 is at most 0.02 for 200 noise realizations when taking the noise amplitude to be 5% of the incoming amplitude of the write pulse. These results confirm the robustness of our approach with respect to possible noise in a real physical system.

IV. CONCLUSION AND OUTLOOK

We have presented a very efficient optimization technique applicable to different experimental realizations based on an inhomogeneously broadened spin ensemble coupled to a single cavity mode. Generalizing this scheme to the full quantum-mechanical level is the obvious next step to make our protocol an essential building block for the development of future optimal control schemes with the perspective of advancing the storage capabilities for quantum information. Given the extremely unfavorable scaling properties of composite quantum systems with particle number, any theoretical description of a quantum many-body system is an extremely challenging task. Since the identification of optimal control strategies is much harder than the mere description of a system's dynamics (the latter is naturally required for the former), optimal control is typically a viable option for rather small systems only. With our highly efficient semiclassical control technique for the non-Markovian dynamics of large hybrid quantum systems in the presence of inhomogeneous broadening, we demonstrate the capabilities and limitations of these systems for potential information storage.

APPENDIX A: VOLTERRA EQUATION FOR THE CAVITY AMPLITUDE

Our starting point is the Hamiltonian (1) of the main text from which we derive the Heisenberg equations for the cavity and spin operators $\dot{a}(t) = i[\mathcal{H}, a(t)] - \kappa a(t)$ and $\dot{\sigma}_k^-(t) = i[\mathcal{H}, \dot{\sigma}_k^-(t)] - \gamma \sigma_k^-(t)$, respectively. Here a stands for the cavity annihilation operator and σ_k^- are standard downward Pauli operators associated with the kth spin; κ and γ are the dissipative cavity and individual spin losses, respectively. (All notation is consistent with that introduced in the main text.) During the derivations we use the following simplifications and approximations valid for various experimental realizations: (i) $k_B T \ll \hbar\omega_c$ (the energy of photons of the external bath $k_B T$ is substantially smaller than that of cavity photons $\hbar\omega_c$); (ii) the number of microwave photons in the cavity remains small as compared to the total number of spins participating in the coupling (limit of low input powers of an incoming signal), so the Holstein-Primakoff-approximation $\langle\sigma_k^{(z)}\rangle \approx -1$ always holds; (iii) the effective collective coupling strength of the spin ensemble $\Omega^2 = \sum_{k=1}^{N} g_k^2$ (g_k stands for the coupling strength of the kth spin) satisfies the inequality $\Omega \ll \omega_c$, justifying the rotating-wave approximation; (iv) the spatial size of the spin ensemble is sufficiently smaller than the wavelength of a cavity mode. Having introduced all these assumptions, we derive the following system of coupled first-order linear ordinary differential equations for the cavity and spin amplitudes in the
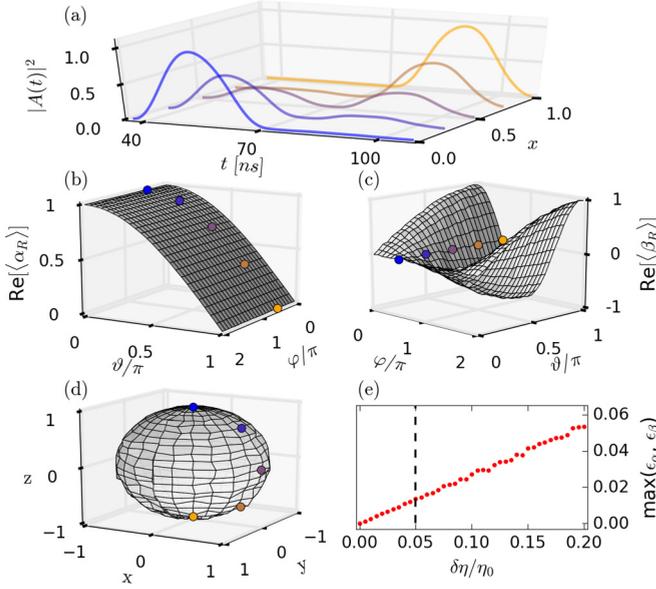
FIG. 3. (a) Retrieved cavity amplitude in the readout section, resulting from a superposition of write pulses $\alpha_x A_{|0\rangle}^{(R)}(t) + \beta_x A_{|1\rangle}^{(R)}(t)$ (normalized to a maximum value of 1) in the absence of noise with the write amplitude $\eta_0 = \kappa$. We used the rebit parametrization α_x and β_x (see the text) from $x = 0$ to 1 in steps of 0.25 (with the same parameters as in Fig. 2, left column). Also shown are the retrieved average values (b) $\langle\alpha_R\rangle$ and (c) $\langle\beta_R\rangle$ (only real parts are shown) from the resulting solution $A^{(R)}(t; \alpha, \beta)$ in the presence of noise. The averaging is performed with respect to 200 noise realizations for a noise amplitude $\delta\eta/\eta_0 = 0.05$. The input configurations are parametrized as $\alpha = \cos(\vartheta/2)$ and $\beta = \sin(\vartheta/2)e^{i\varphi}$ with $\vartheta \in [0,\pi]$ and $\varphi \in [0,2\pi]$. (d) Reconstructed Bloch sphere with spatial components $r_i = (\langle\alpha_R\rangle^*, \langle\beta_R\rangle^*)\sigma_i(\langle\alpha_R\rangle, \langle\beta_R\rangle)$ for $i = x, y, z$, evaluated from the retrieved averaged parameters taken from (b) and (c), where σ_i is the ith Pauli matrix. The symbols in (b)–(d) emphasize the rebit encoding from (a). The reference configurations $|0/1\rangle$ are taken from the left column of Fig. 2. (e) Maximum of the absolute errors $\epsilon_\alpha = |\alpha - \langle\alpha_R\rangle|$ and $\epsilon_\beta = |\beta - \langle\beta_R\rangle|$ in retrieval of the input configurations for different noise amplitudes $\delta\eta$. Vertical dashed line shows the noise level of the calculations in (b)–(d).

ω_p-rotating frame:

$$\dot{A}(t) = -[\kappa + i\Delta_c]A(t) + \sum_{k=1}^{N} g_k B_k(t) - \eta(t), \quad \text{(A1)}$$

$$\dot{B}_k(t) = -[\gamma + i\Delta_k]B_k(t) - g_k A(t), \quad \text{(A2)}$$

where $A(t) \equiv \langle a(t)\rangle$ and $B_k(t) \equiv \langle\sigma_k^-(t)\rangle$. In addition, $\Delta_c = \omega_c - \omega_p$ and $\Delta_k = \omega_k - \omega_p$ are the detunings with respect to the probe frequency ω_p.

By formally integrating Eq. (A2) with respect to time for the spin operators and inserting them into Eq. (A1) for the cavity operator, we get

$$\dot{A}(t) = -[\kappa + i\Delta_c]A(t) + \sum_{k=1}^{N} g_k B_k(T_1)\, e^{-[\gamma + i\Delta_k](t-T_1)}$$

$$- \Omega^2 \int_0^\infty d\omega\, \rho(\omega) \int_{T_1}^t d\tau\, A(\tau)e^{-[\gamma + i\Delta_\omega](t-\tau)} - \eta(t),$$

$$\text{(A3)}$$

where $\Delta_\omega = \omega - \omega_p$, $B_k(T_1)$ is the initial spin amplitude at $t = T_1$, and $\rho(\omega) = \sum_{k=1}^{N} g_k^2 \delta(\omega - \omega_k)/\Omega^2$ stands for the continuous spectral spin distribution. As in our previous studies [29,36], we take into account the effect of an inhomogeneous broadening by modeling the spin density with a q-Gaussian shape $\rho(\omega) = C[1 - (1 - q)(\omega - \omega_s)^2/\Delta^2]^{1/(1-q)}$, distributed around the mean frequency $\omega_s/2\pi = 2.6915$ GHz with the parameter $q = 1.39$ and a full width at half maximum $\gamma_q/2\pi = 9.4$ MHz, where $\gamma_q = 2\Delta\sqrt{(2^q - 2)/(2q - 2)}$.

Next we formally integrate Eq. (A3) in time and simplify the resulting double integral on the right-hand side by partial integration. We also consider the case when the cavity is initially empty $A(T_1) = 0$ and all spins are in the ground state $B_k(T_1) = 0$. To speed up our numerical calculations and to separate different time sections from each other (see the main text and Appendix B for details), we divide the whole time integration into successive subintervals $T_n \leqslant t \leqslant T_{n+1}$, with $n = 1, 2, \ldots$ (see Fig. 4). This allows us to derive the recurrence relation for the cavity amplitude for the nth time interval $A^{(n)}(t)$, which depends on all previous events at $t < T_n$. Finally, we end up with the expression for $A^{(n)}(t)$,

$$A^{(n)}(t) = \int_{T_n}^t d\tau\, \mathcal{K}(t - \tau)A^{(n)}(\tau) + \mathcal{D}^{(n)}(t) + \mathcal{F}^{(n)}(t), \quad \text{(A4)}$$

where the non-Markovian feedback within the nth time interval is provided by the kernel function $\mathcal{K}(t - \tau)$,

$$\mathcal{K}(t - \tau) = \Omega^2 \int_0^\infty d\omega\, \rho(\omega) \frac{e^{-[\gamma + i\Delta_\omega](t-\tau)} - e^{[\kappa + i\Delta_c](t-\tau)}}{[\gamma + i\Delta_\omega] - [\kappa + i\Delta_c]}.$$

$$\text{(A5)}$$

The driving term $\mathcal{D}^{(n)}(t)$ in Eq. (A4),

$$\mathcal{D}^{(n)}(t) = -\int_{T_n}^t d\tau\, \eta^{(n)}(\tau)e^{-[\kappa + i\Delta_c](t-\tau)}, \quad \text{(A6)}$$

includes an arbitrarily shaped, weak incoming pulse $\eta^{(n)}(t)$, defined in the time interval $[T_n, T_{n+1}]$. The memory contributions from all previous time intervals for $t < T_n$ are given both through the amplitude $A^{(n-1)}(T_n)$ and through the memory

FIG. 4. Schematics of the time divisions of the cavity amplitude $A^{(n)}(t)$. The input field $\eta^{(n)}(t)$ is applied to the system in the time interval $[T_n, T_{n+1}]$ and drives the corresponding cavity amplitude $A^{(n)}(t)$ (indicated by vertical arrows). The non-Markovian contributions from previous time intervals $[T_{n-1}, T_n]$ are indicated by horizontal arrows.

integral $\mathcal{I}^{(n)}(\omega)$, which are contained in the function

$$\mathcal{F}^{(n)}(t) = \left\{ A^{(n-1)}(T_n)e^{-[\kappa+i\Delta_c](t-T_n)} + \Omega^2 \int_0^\infty d\omega \, \rho(\omega) \frac{e^{-[\gamma+i\Delta(\omega)](t-T_n)} - e^{-[\kappa+i\Delta_c](t-T_n)}}{[\gamma+i\Delta_\omega]-[\kappa+i\Delta_c]} \mathcal{I}^{(n)}(\omega) \right\}, \tag{A7}$$

where

$$\mathcal{I}^{(n)}(\omega) = \mathcal{I}^{(n-1)}(\omega)e^{-[\gamma+i\Delta_\omega](T_n-T_{n-1})} + \int_{T_{n-1}}^{T_n} d\tau \, A^{(n-1)}(\tau)e^{-[\gamma+i\Delta_\omega](T_n-\tau)}. \tag{A8}$$

In accordance with the initial conditions introduced above at $t = T_1$, $A^{(0)}(T_1) = 0$ and $\mathcal{I}^{(1)}(\omega) = 0$, so $\mathcal{F}^{(1)}(t)$ vanishes in the first time interval $\mathcal{F}^{(1)}(t) = 0$ $(T_1 \leqslant t \leqslant T_2)$.

APPENDIX B: OPTIMAL CONTROL BASED ON THE VOLTERRA EQUATION

In the main text we split our time interval into two parts, a write and readout section, with a variable delay section in between. In the write section, two independent optimized write pulses $\eta^{(W)}(t)$ prepare two different configurations of the spin ensemble, which are referred to as logical states $|0\rangle$ and $|1\rangle$ of the spin ensemble. It is followed by the delay section characterized by almost completely suppressed cavity responses and finally by the readout section where two logical states of the spin ensemble are retrieved and mapped on two mutually orthogonal states of the cavity field by means of the readout pulse $\eta^{(R)}(t)$ (see Fig. 5). Note that the optimized readout pulse is generic, being the same for both $|0\rangle$ and $|1\rangle$ states. For the sake of simplicity, we do not explicitly specify the delay pulse but impose on the readout pulse $\eta^{(R)}(t)$ a constraint such that the cavity responses are maximally suppressed in the delay section $[T_2, \tau_a]$ (see Fig. 5). Thus, the write and readout pulses are defined within the time intervals $[T_1, T_2]$ and $[T_2, T_3]$, respectively, in terms of the notations introduced in Appendix A and the delay section is formally absorbed into the readout section.

We then expand $\eta^{(W)}(t)$ and $\eta^{(R)}(t)$ in terms of sine functions

$$\eta^{(W)}(t) = \sum_{k=1}^{N_1} \xi_k \sin[k\omega_f(t-T_1)], \tag{B1}$$

$$\eta^{(R)}(t) = \sum_{l=1}^{N_2} \zeta_l \sin[l\omega_f(t-T_2)], \tag{B2}$$
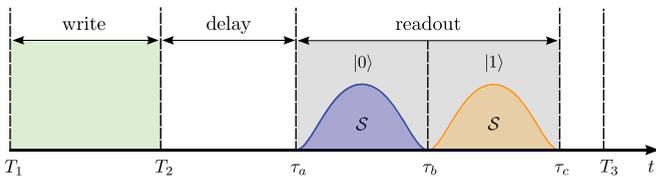
FIG. 5. Time divisions for the optimization scheme of the cavity responses $A_{|0\rangle}^{(R)}(t)$ and $A_{|1\rangle}^{(R)}(t)$. The write section $[T_1, T_2]$ is followed by the variable delay section $[T_2, \tau_a]$ and the readout section $[\tau_a, \tau_c]$. The cavity responses $A_{|0\rangle}^{(R)}(t)$ and $A_{|1\rangle}^{(R)}(t)$ reside in the first half $[\tau_a, \tau_b]$ and the second half $[\tau_b, \tau_c]$ of the readout section, respectively.

where ξ_k and ζ_l are the expansion coefficients and ω_f is the fundamental frequency. The linear property of the Volterra equation (A4) allows us to expand the cavity amplitude in the write section $A^{(W)}(t)$ in a series of time-dependent functions with the same expansion coefficients ξ_k as in Eq. (B1),

$$A^{(W)}(t) = \sum_{k=1}^{N_1} \xi_k a_k^{(W)}(t). \tag{B3}$$

Here $a_k^{(W)}(t)$ are solutions of the Volterra equation

$$a_k^{(W)}(t) = \int_{T_1}^t d\tau \, K(t-\tau)a_k^{(W)}(\tau)$$
$$- \int_{T_1}^t d\tau \, \sin[k\omega_f(\tau-T_1)]e^{-[\kappa+i\Delta_c](t-\tau)}, \tag{B4}$$

where the kernel function $\mathcal{K}(t-\tau)$ is given by Eq. (A5).

The solution in the readout section $A^{(R)}(t)$ in turn consists of two contributions

$$A^{(R)}(t) = \sum_{l=1}^{N_2} \zeta_l a_l^{(R)}(t) + \sum_{k=1}^{N_1} \xi_k \psi_k^{(R)}(t). \tag{B5}$$

Similar to the ansatz for the write section, the first term in Eq. (B5) also contains the same expansion coefficients ζ_l as the corresponding driving signal in the readout section [see Eq. (B2)] with the time-dependent functions $a_l^{(R)}(t)$ obeying the Volterra equation $(T_2 \leqslant t \leqslant T_3)$

$$a_l^{(R)}(t) = \int_{T_2}^t d\tau \, \mathcal{K}(t-\tau)a_l^{(R)}(\tau)$$
$$- \int_{T_2}^t d\tau \, \sin[l\omega_f(\tau-T_2)]e^{-[\kappa+i\Delta_c](t-\tau)}. \tag{B6}$$

Additionally, the second term in Eq. (B5) describes the non-Markovian memory and appears in the readout section due to the energy stored in both the cavity and spin ensemble during the time interval $T_1 \leqslant t \leqslant T_2$ (write section). Therefore, it depends only on the coefficients ξ_k of the write pulse (B1) and the time-dependent functions $\psi_k^{(R)}(t)$, which can be found by substituting the expressions (B3) and (B5) into Eqs. (A4)–(A8) for $n = 2$. It can be shown that these functions satisfy the Volterra equation

$$\psi_k^{(R)}(t) = \int_{T_2}^t d\tau \, \mathcal{K}(t-\tau)\psi_k^{(R)}(\tau) + f_k^{(R)}(t), \tag{B7}$$

with the feedback from the previous write section defined by

$$f_k^{(R)}(t) = a_k^{(W)}(T_2)e^{-[\kappa+i\Delta_c](t-T_2)} + \Omega^2 \int_0^\infty d\omega\, \rho(\omega) \frac{e^{-[\gamma+i\Delta_\omega](t-T_2)} - e^{-[\kappa+i\Delta_c](t-T_2)}}{[\gamma+i\Delta_\omega] - [\kappa+i\Delta_c]} \int_{T_1}^{T_2} d\tau\, a_k^{(W)}(\tau)e^{-[\gamma+i\Delta_\omega](T_2-\tau)}. \quad \text{(B8)}$$

Note that the $a_k^{(W)}(t)$ in Eq. (B8) are defined in the write section only and are known solutions of Eq. (B4).

In the main text we use two different pulses $\eta_{|0\rangle}^{(W)}(t) = \sum_{k=1}^{N_1} \xi_k^{|0\rangle} \sin[k\omega_f(t-T_1)]$ and $\eta_{|1\rangle}^{(W)}(t) = \sum_{k=1}^{N_1} \xi_k^{|1\rangle} \sin[k\omega_f(t-T_1)]$ in the write section, which are characterized by two sets of expansion coefficients from Eq. (B1). As a result, the cavity amplitudes in the write section are also represented by these sets of expansion coefficients and are given by Eq. (B3), namely,

$$A_{|0\rangle}^{(W)}(t) = \sum_{k=1}^{N_1} \xi_k^{|0\rangle} a_k^{(W)}(t),$$

$$A_{|1\rangle}^{(W)}(t) = \sum_{k=1}^{N_1} \xi_k^{|1\rangle} a_k^{(W)}(t). \quad \text{(B9)}$$

Note that by injecting these pulses into the cavity, we create two independent configurations (denoted by $|0\rangle$ and $|1\rangle$) of the spin-cavity system at the beginning of the readout interval $t = T_2$.

Next we perform a readout by applying a single optimized readout pulse (B2), which is the same for the states $|0\rangle$ and $|1\rangle$. The cavity amplitudes in the readout section in turn are governed by Eq. (B5) as

$$A_{|0\rangle}^{(R)}(t) = \underbrace{\sum_{l=1}^{N_2} \zeta_l a_l^{(R)}(t)}_{\tilde{A}^{(R)}(t)} + \underbrace{\sum_{k=1}^{N_1} \xi_k^{|0\rangle} \psi_k^{(R)}(t)}_{\tilde{A}_{|0\rangle}^{(R)}(t)},$$

$$A_{|1\rangle}^{(R)}(t) = \underbrace{\sum_{l=1}^{N_2} \zeta_l a_l^{(R)}(t)}_{\tilde{A}^{(R)}(t)} + \underbrace{\sum_{k=1}^{N_1} \xi_k^{|1\rangle} \psi_k^{(R)}(t)}_{\tilde{A}_{|1\rangle}^{(R)}(t)}, \quad \text{(B10)}$$

where $\tilde{A}^{(R)}(t)$ describes the contribution from the readout pulse only, which is the same for both cavity responses and the two other terms $\tilde{A}_{|i\rangle}^{(R)}(t)$ ($i = 0, 1$) explicitly depend on the states $|0\rangle$ and $|1\rangle$ created in the write section. Thus, the cavity amplitude is determined at every moment of time by Eqs. (B3)–(B8) (and, as a consequence, all spin configurations), if all expansion coefficients $\xi_k^{|0\rangle}$, $\xi_k^{|1\rangle}$, and ζ_l are provided.

As the next step we develop an optimization scheme aiming at achieving two well-resolved cavity responses in the readout section, $A_{|0\rangle}^{(R)}(t)$ and $A_{|1\rangle}^{(R)}(t)$, as is sketched in Fig. 5. (The results of numerical calculations are presented in Fig. 2.) For this purpose we use the standard method of Lagrange multipliers by introducing the functional $\mathcal{F}(\xi_k^{|0\rangle}, \xi_k^{|1\rangle}, \zeta_l)$ subject to several constraints listed below and search for its minima with respect to the expansion coefficients of all three pulses.

Namely, we write the expression for the functional

$$\mathcal{F}(\xi_k^{|0\rangle}, \xi_k^{|1\rangle}, \zeta_l) = \int_{\tau_b}^{\tau_c} dt |A_{|0\rangle}^{(R)}(t)|^2 + \int_{\tau_a}^{\tau_b} dt |A_{|1\rangle}^{(R)}(t)|^2$$

$$+ \left| \int_{\tau_a}^{\tau_c} dt\, A_{|0\rangle}^{(R)\star}(t) A_{|1\rangle}^{(R)}(t) \right|$$

$$- \lambda_{\text{delay}}^{|0\rangle} \int_{T_2}^{\tau_a} dt |A_{|0\rangle}^{(R)}(t)|^2 - \lambda_{\text{delay}}^{|1\rangle}$$

$$\times \int_{T_2}^{\tau_a} dt |A_{|1\rangle}^{(R)}(t)|^2 - \lambda_T^{|0\rangle} |A_{|0\rangle}^{(R)}(\tau_a)|^2$$

$$- \lambda_T^{|1\rangle} \left| A_{|1\rangle}^{(R)}(\tau_a) \right|^2 - \lambda_{\Delta T}^{|0\rangle}$$

$$\times \left(\int_{\tau_a}^{\tau_b} dt \left| A_{|0\rangle}^{(R)}(t) \right|^2 - \mathcal{S} \right)$$

$$- \lambda_{\Delta T}^{|1\rangle} \left(\int_{\tau_b}^{\tau_c} dt \left| A_{|1\rangle}^{(R)}(t) \right|^2 - \mathcal{S} \right)$$

$$- \lambda_P^{|0\rangle} \left(\sum_k \left| \xi_k^{|0\rangle} \right|^2 - \mathcal{P} \right)$$

$$- \lambda_P^{|1\rangle} \left(\sum_k \left| \xi_k^{|1\rangle} \right|^2 - \mathcal{P} \right), \quad \text{(B11)}$$

where the λ are the Lagrange multipliers. The first three terms in Eq. (B11) are the functions to be minimized, which ensure that the overlap between the time-binned states in the readout section is negligibly small. The rest of the terms are constraints, which additionally guarantee the following conditions to be simultaneously fulfilled: (i) The cavity responses within the delay section are maximally suppressed; (ii) the cavity at the beginning of the readout section is almost empty for both states; (iii) the integral taken with respect to the time-binned cavity amplitudes squared within the readout section has the same value $\mathcal{S}$; (iv) a net power $\mathcal{P}$ of the write pulses per fundamental period $2\pi/\omega_f$ is the same. In our numerical calculations we used the sequential least-squares programming minimization method [41] embedded in the internal python library SCIPY.OPTIMIZE to find the minima of the functional $\mathcal{F}(\xi_k^{|0\rangle}, \xi_k^{|1\rangle}, \zeta_l)$.

In the main text we created an arbitrary superposition of write pulses (each of which separately prepares the logical state $|0\rangle$ or $|1\rangle$) by applying the superimposed write pulse

$$\eta^{(W)}(t) = \alpha \eta_{|0\rangle}^{(W)}(t) + \beta \eta_{|1\rangle}^{(W)}(t), \quad \text{(B12)}$$

aiming to extract the encoded information (given by complex numbers α and β) from the solution for the cavity amplitude in the readout section designated in Fig. 5. [Note that the reading pulse $\eta^{(R)}(t)$ is always kept the same.] The solution in the readout section can be written as

$$A^{(R)}(t; \alpha, \beta) = \alpha \tilde{A}_{|0\rangle}^{(R)}(t) + \beta \tilde{A}_{|1\rangle}^{(R)}(t) + \tilde{A}^{(R)}(t), \quad \text{(B13)}$$

with all three previously established well-known amplitudes $\tilde{A}_{|0\rangle}^{(R)}(t)$, $\tilde{A}_{|1\rangle}^{(R)}(t)$, and $\tilde{A}^{(R)}(t)$ introduced in Eq. (B10). We then project our resulting solution (B13) onto the functions $A_{|0\rangle}^{(R)}(t)$ and $A_{|1\rangle}^{(R)}(t)$ from Eq. (B10), namely, we write

$$\mathcal{O}_i = \int_{\tau_a}^{\tau_c} dt\, A^{(R)}(t;\alpha,\beta) A_{|i\rangle}^{(R)*}(t)$$
$$= \alpha \mathcal{F}_{i,0} + \beta \mathcal{F}_{i,1} + \mathcal{F}_{i,R}, \qquad (B14)$$

where the overlap integrals $\mathcal{F}_{i,q} = \int_{\tau_a}^{\tau_c} dt\, \tilde{A}_{|q\rangle}^{(R)}(t) A_{|i\rangle}^{(R)*}(t)$ with $i,q = 0,1$ and $\mathcal{F}_{i,R} = \int_{\tau_a}^{\tau_c} dt\, \tilde{A}^{(R)}(t) A_{|i\rangle}^{(R)*}(t)$. Since $\mathcal{F}_{i,q}$ and $\mathcal{F}_{i,R}$ are known we finally end up with the set of two algebraic equations

$$\mathcal{O}_0 = \alpha \mathcal{F}_{0,0} + \beta \mathcal{F}_{0,1} + \mathcal{F}_{0,R}, \qquad (B15)$$

$$\mathcal{O}_1 = \alpha \mathcal{F}_{1,0} + \beta \mathcal{F}_{1,1} + \mathcal{F}_{1,R}, \qquad (B16)$$

from which the retrieved values α_R and β_R can be evaluated.

APPENDIX C: RETRIEVAL OF ENCODED PARAMETERS IN THE PRESENCE OF NOISE

Here we study the influence of noise on the quality of our optimization scheme presented in the main text and introduced in Appendix B. For that purpose, we subject the previously established optimal driving amplitudes $\eta_{|0\rangle}^{(W)}(t)$, $\eta_{|1\rangle}^{(W)}(t)$, and $\eta^{(R)}(t)$ (see Appendix B) to a small perturbation represented by the driving term $\delta\eta_{\text{noise}}(t) = \delta\eta\, \upsilon(t)$, where $\delta\eta$ is the amplitude of perturbation and $\upsilon(t)$ stands for a Gaussian white noise of mean and correlations given by, respectively, $\langle \upsilon(t)\rangle = 0$ and $\langle \upsilon(t')\upsilon(t)\rangle = \delta(t - t')$. We then numerically integrate the Volterra equation (A3) from Appendix A with respect to time by adding the perturbation $\delta\eta_{\text{noise}}(t)$ to the corresponding deterministic optimal driving amplitudes $\eta(t)$, which in our specific case are represented by the known writing and readout amplitudes $\eta_{|0\rangle}^{(W)}(t)$, $\eta_{|1\rangle}^{(W)}(t)$, and $\eta^{(R)}(t)$. We treat the problem numerically using well-established numerical methods for integrating stochastic differential equations (see, e.g., [40]). Concisely, the stochastic contribution to the cavity amplitude is taken into account after each time step of numerical integration in the following way: $A(t_{m+1}) \to A(t_{m+1}) + \sqrt{dt}\,\delta\eta_{\text{noise}}(t_m)$, where $A(t_{m+1})$ after the arrow corresponds to the deterministic part of the cavity amplitude at $t = t_{m+1}$ obtained using the standard Runge-Kutta method and $\delta\eta_{\text{noise}}(t_m)$ is the stochastic drive taken from the previous time step. We then accumulate statistics by integrating many trajectories for different noise

realizations. Next we extract the encoded parameters $\alpha_{\mathcal{R}}$ and $\beta_{\mathcal{R}}$ in the presence of noise replacing the overlap integrals in Eqs. (B15) and (B16) for the case without noise by the corresponding overlap integrals evaluated for different noise realizations. The result of calculations for the average retrieval values of $\langle \alpha_{\mathcal{R}}\rangle$ and $\langle \beta_{\mathcal{R}}\rangle$ and their absolute errors $\epsilon_\alpha = |\alpha - \langle \alpha_{\mathcal{R}}\rangle|$ and $\epsilon_\beta = |\beta - \langle \beta_{\mathcal{R}}\rangle|$ with respect to the encoded values are depicted in Fig. 3.

APPENDIX D: NUMERICAL VALUES FOR THE OPTIMIZED READOUT PULSE COEFFICIENTS

Here we present numerical values of the coefficients $\xi_k^{|0\rangle}$, $\xi_k^{|1\rangle}$, and ζ_l of the optimal readout pulses $\eta_{|0\rangle}^{(W)}(t)$, $\eta_{|1\rangle}^{(W)}(t)$, and $\eta^{(R)}(t)$ defined by Eqs. (B1) and (B2), which are presented in the main text. We take the amplitude of the write pulses such that the net power injected into the cavity $\mathcal{P}_{|i\rangle}^{(W)} = \frac{1}{T_f} \int_0^{T_f} dt |\eta_{|i\rangle}^{(W)}(t)|^2 = \kappa^2$, with $i = 0,1$, such that it corresponds to the power provided by a coherent driving signal with the amplitude equal to the cavity decay rate $\eta = \kappa$. Specifically, using the expansion (B1) for the write pulses $\eta^{(W)}(t)$, we obtain the following expression for the power of the write pulses per fundamental period T_f:

$$\mathcal{P}_{|i\rangle}^{(W)} = \eta^{(W)2} \frac{1}{2} \sum_{k=1}^{N_1} |\xi_k^{|i\rangle}/\eta^{(W)}|^2 = \kappa^2, \qquad (D1)$$

where $\eta^{(W)} = \kappa$ and $\frac{1}{2}\sum_{k=1}^{N_1} |\xi_k^{|i\rangle}/\kappa|^2 = 1$ due to the constraint imposed on the expansion coefficients. On the other hand, the power of the readout pulse is substantially smaller than that of the write pulses and for the case without hole burning (see left column of Fig. 2) we obtain

$$\mathcal{P}^{(R)} = \eta^{(R)2} \frac{1}{2} \sum_{k=1}^{N_2} |\zeta_l/\eta^{(R)}|^2 = 0.068\kappa^2, \qquad (D2)$$

where $\eta^{(R)} = 0.26\kappa$ and again we use as the constraint $\frac{1}{2}\sum_{l=1}^{N_2} |\zeta_l/\eta^{(R)}|^2 = 1$.

The coefficients for all optimal readout pulses shown in the left column of Fig. 2 are listed in Table I. For the sake of convenience, the coefficients of the write and readout pulses are normalized to $\eta^{(W)}$ and $\eta^{(R)}$, respectively. We use $N_1 = 5$ coefficients for the write pulse and $N_2 = 10$ for the readout pulse (notation is consistent with that used in Appendices A and B). The fundamental frequency for the write pulses is given by $\omega_f = \pi/(T_2 - T_1) = \Omega_R$ and for the readout pulse we use $\omega_f = \pi/(T_3 - T_2) = \Omega_R/2$. Here the Rabi frequency $\Omega_R = 2\pi \times 13.62$ MHz and the time divisions shown in Fig. 5

TABLE I. Normalized expansion coefficients $\xi_{k=1,...,5}^{|i\rangle}$ (for $i = 0,1$) and $\zeta_{k=1,...,10}$ defined by Eqs. (B1) and (B2), which correspond to the optimal readout pulses $\eta_{|0\rangle}^{(W)}(t)$, $\eta_{|1\rangle}^{(W)}(t)$, and $\eta^{(R)}(t)$ depicted in the left column of Fig. 2. The coefficients for the write pulses are normalized to $\eta^{(W)} = \kappa$ and for the readout pulse to $\eta^{(R)} = 0.26\kappa$.

$\xi_{k=1,...,5}^{|0\rangle}$	$\xi_{k=1,...,5}^{|1\rangle}$	$\zeta_{l=1,...,5}$	$\zeta_{l=6,...,10}$
$0.434 + 0.103i$	$-0.043 - 0.013i$	$-1.003 - 0.250i$	$0.229 + 0.054i$
$0.303 + 0.067i$	$-0.231 - 0.055i$	$0.820 + 0.195i$	$0.037 + 0.007i$
$1.060 + 0.259i$	$-1.127 - 0.273i$	$-0.017 - 0.007i$	$-0.096 - 0.025i$
$-0.152 - 0.023i$	$0.200 + 0.044i$	$-0.213 - 0.054i$	$-0.174 - 0.043i$
$0.682 + 0.161i$	$-0.723 - 0.175i$	$-0.243 - 0.061i$	$0.105 + 0.024i$

TABLE II. Normalized expansion coefficients $\xi_{k=1,\ldots,4}^{|i\rangle}$ (for $i = 0, 1$) and $\zeta_{k=1,\ldots,60}$ defined by Eqs. (B1) and (B2), which correspond to the optimal readout pulses $\eta_{|0\rangle}^{(W)}(t)$, $\eta_{|1\rangle}^{(W)}(t)$, and $\eta^{(R)}(t)$ depicted in the right column of Fig. 2. The coefficients for the write pulses are normalized to $\eta^{(W)} = \kappa$ and for the readout pulse to $\eta^{(R)} = 0.11\kappa$.

$\xi_{k=1,\ldots,4}^{|0\rangle}$	$\xi_{k=1,\ldots,4}^{|1\rangle}$	$\zeta_{l=1,\ldots,15}$	$\zeta_{l=16,\ldots,30}$	$\zeta_{l=31,\ldots,45}$	$\zeta_{l=46,\ldots,60}$
$-0.227 + 0.108i$	$1.252 - 0.161i$	$0.066 - 0.028i$	$-0.239 - 0.024i$	$0.054 - 0.032i$	$-0.036 - 0.010i$
$0.017 + 0.046i$	$0.074 + 0.050i$	$-0.121 - 0.022i$	$0.228 - 0.088i$	$-0.041 - 0.014i$	$0.059 - 0.021i$
$1.014 - 0.161i$	$-0.243 + 0.083i$	$0.190 - 0.128i$	$-0.170 - 0.013i$	$0.044 - 0.029i$	$-0.069 - 0.011i$
$0.938 - 0.032i$	$0.574 + 0.040i$	$-0.230 + 0.010i$	$0.161 - 0.080i$	$-0.027 - 0.014i$	$0.090 - 0.026i$
		$0.292 - 0.151i$	$-0.109 - 0.019i$	$0.027 - 0.025i$	$-0.096 - 0.007i$
		$-0.313 + 0.033i$	$0.107 - 0.059i$	$-0.007 - 0.015i$	$0.112 - 0.040i$
		$0.365 - 0.155i$	$-0.066 - 0.020i$	$0.006 - 0.020i$	$-0.112 + 0.016i$
		$-0.363 + 0.028i$	$0.073 - 0.051i$	$0.012 - 0.020i$	$0.122 - 0.051i$
		$0.398 - 0.160i$	$-0.042 - 0.021i$	$-0.009 - 0.017i$	$-0.118 + 0.004i$
		$-0.377 - 0.001i$	$0.058 - 0.044i$	$0.021 - 0.022i$	$0.122 - 0.033i$
		$0.395 - 0.136i$	$-0.032 - 0.021i$	$-0.012 - 0.009i$	$-0.115 + 0.011i$
		$-0.355 - 0.009i$	$0.025 - 0.040i$	$0.016 - 0.021i$	$0.117 - 0.031i$
		$0.358 - 0.097i$	$-0.085 - 0.017i$	$0.000 - 0.014i$	$-0.108 + 0.001i$
		$-0.305 - 0.001i$	$0.049 - 0.033i$	$-0.004 - 0.018i$	$0.107 - 0.032i$
		$0.298 - 0.093i$	$-0.047 - 0.015i$	$0.026 - 0.023i$	$-0.095 + 0.020i$

are $T_1 = 0$, $T_2 = 36.72$ ns, and $T_3 = 110.15$ ns. The readout section $[\tau_a, \tau_c]$ coincides with the whole readout interval $[T_2, T_3]$.

For the case with hole burning, depicted in the right column of Fig. 2, we use $N_1 = 4$ and $N_2 = 60$. All coefficients are summarized in Table II. Here we choose the fundamental frequency for the write pulses as $\omega_f = \pi/(T_2 - T_1) = \Omega_R/2$, whereas $\omega_f = \pi/(T_3 - T_2) = \Omega_R/30$ for the readout pulse. The time divisions are $T_1 = 0$, $T_2 = 73.4$ ns, and $T_3 = 1174.9$ ns and the Rabi frequency $\Omega_R = 2\pi \times 13.62$ MHz. The readout section defined by $\tau_a = 1114.3$ ns and $\tau_c = 1153.6$ ns is delayed by approximately 1 μs with respect to the write section $[T_1, T_2]$. The power ratio of the readout pulse to the write pulse turns out to be $\mathcal{P}^{(R)}/\mathcal{P}^{(W)} = 0.013$.

[1] T. P. Harty, D. T. C. Allcock, C. J. Ballance, L. Guidoni, H. A. Janacek, N. M. Linke, D. N. Stacey, and D. M. Lucas, Phys. Rev. Lett. **113**, 220501 (2014).

[2] J. L. O'Brien, G. J. Pryde, A. G. White, T. C. Ralph, and D. Branning, Nature (London) **426**, 264 (2003).

[3] J. H. Plantenberg, P. C. de Groot, C. J. P. M. Harmans, and J. E. Mooij, Nature (London) **447**, 836 (2007).

[4] P. J. J. O'Malley *et al.*, Phys. Rev. X **6**, 031007 (2016).

[5] P. Macha, G. Oelsner, J.-M. Reiner, M. Marthaler, S. André, G. Schön, U. Hübner, H.-G. Meyer, E. Il'ichev, and A. V. Ustinov, Nat. Commun. **5**, 5146 (2014).

[6] K. V. Shulga, P. Yang, G. P. Fedorov, M. V. Fistul, M. Weides, and A. V. Ustinov, JETP Lett. **105**, 47 (2017).

[7] P. L. Stanwix, L. M. Pham, J. R. Maze, D. Le Sage, T. K. Yeung, P. Cappellaro, P. R. Hemmer, A. Yacoby, M. D. Lukin, and R. L. Walsworth, Phys. Rev. B **82**, 201201(R) (2010).

[8] R. Amsüss, C. Koller, T. Nöbauer, S. Putz, S. Rotter, K. Sandner, S. Schneider, M. Schramböck, G. Steinhauser, H. Ritsch, J. Schmiedmayer, and J. Majer, Phys. Rev. Lett. **107**, 060502 (2011).

[9] Y. Kubo *et al.*, Phys. Rev. Lett. **105**, 140502 (2010).

[10] S. Probst, H. Rotzinger, S. Wünsch, P. Jung, M. Jerger, M. Siegel, A. V. Ustinov, and P. A. Bushev, Phys. Rev. Lett. **110**, 157001 (2013).

[11] P. Rabl, D. DeMille, J. M. Doyle, M. D. Lukin, R. J. Schoelkopf, and P. Zoller, Phys. Rev. Lett. **97**, 033003 (2006).

[12] M. Afzelius, C. Simon, H. de Riedmatten, and N. Gisin, Phys. Rev. A **79**, 052329 (2009).

[13] J. Verdú, H. Zoubi, C. Koller, J. Majer, H. Ritsch, and J. Schmiedmayer, Phys. Rev. Lett. **103**, 043603 (2009).

[14] S. A. Moiseev and S. Kröll, Phys. Rev. Lett. **87**, 173601 (2001).

[15] W. Tittel, M. Afzelius, T. Chaneliere, R. L. Cone, S. Kröll, S. A. Moiseev, and M. Sellars, Laser Photon. Rev. **4**, 244 (2010).

[16] B. Kraus, W. Tittel, N. Gisin, M. Nilsson, S. Kröll, and J. I. Cirac, Phys. Rev. A **73**, 020302(R) (2006).

[17] B. Julsgaard and K. Mølmer, Phys. Rev. A **88**, 062324 (2013).

[18] C. Grezes *et al.*, Phys. Rev. X **4**, 021049 (2014).

[19] N. Gisin, S. A. Moiseev, and C. Simon, Phys. Rev. A **76**, 014302 (2007).

[20] M. U. Staudt, S. R. Hastings-Simon, M. Nilsson, M. Afzelius, V. Scarani, R. Ricken, H. Suche, W. Sohler, W. Tittel, and N. Gisin, Phys. Rev. Lett. **98**, 113601 (2007).

[21] H. de Riedmatten, M. Afzelius, M. U. Staudt, C. Simon, and N. Gisin, Nature (London) **456**, 773 (2008).

[22] M. Gündogan, P. M. Ledingham, K. Kutluer, M. Mazzera, and H. de Riedmatten, Phys. Rev. Lett. **114**, 230501 (2015).

[23] P. Jobez, I. Usmani, N. Timoney, C. Laplane, N. Gisin, and M. Afzelius, New J. Phys. **16**, 083005 (2014).

[24] S. A. Moiseev and J.-L. Le Gouët, J. Phys. B **45**, 124003 (2012).

[25] I. Novikova, N. B. Phillips, and A. V. Gorshkov, Phys. Rev. A **78**, 021802(R) (2008).

[26] D. O. Krimer, B. Hartl, and S. Rotter, Phys. Rev. Lett. **115**, 033601 (2015).

[27] S. Putz, A. Angerer, D. O. Krimer, R. Glattauer, W. J. Munro, S. Rotter, J. Schmiedmayer, and J. Majer, Nat. Photon. **11**, 36 (2017).

[28] D. O. Krimer, M. Zens, S. Putz, and S. Rotter, Laser Photon. Rev. **10**, 1023 (2016).

[29] S. Putz, D. O. Krimer, R. Amsüss, A. Valookaran, T. Nöbauer, J. Schmiedmayer, S. Rotter, and J. Majer, Nat. Phys. **10**, 720 (2014).

[30] C. U. Lei and W.-M. Zhang, Ann. Phys. (NY) **327**, 1408 (2012).

[31] W.-M. Zhang, P.-Y. Lo, H.-N. Xiong, M. W.-Y. Tu, and F. Nori, Phys. Rev. Lett. **109**, 170402 (2012).

[32] M. Tavis and F. W. Cummings, Phys. Rev. **170**, 379 (1968).

[33] K. Sandner, H. Ritsch, R. Amsüss, C. Koller, T. Nöbauer, S. Putz, J. Schmiedmayer, and J. Majer, Phys. Rev. A **85**, 053806 (2012).

[34] J. Brendel, N. Gisin, W. Tittel, and H. Zbinden, Phys. Rev. Lett. **82**, 2594 (1999).

[35] H. Primakoff and T. Holstein, Phys. Rev. **55**, 1218 (1939).

[36] D. O. Krimer, S. Putz, J. Majer, and S. Rotter, Phys. Rev. A **90**, 043852 (2014).

[37] I. Diniz, S. Portolan, R. Ferreira, J. M. Gérard, P. Bertet, and A. Aufféves, Phys. Rev. A **84**, 063810 (2011).

[38] Z. Kurucz, J. H. Wesenberg, and K. Mølmer, Phys. Rev. A **83**, 053852 (2011).

[39] J. Batle, A. R. Plastino, M. Casas, and A. Plastino, Opt. Spectrosc. **94**, 700 (2003).

[40] R. Toral and P. Colet, *Stochastic Numerical Methods: An Introduction for Students and Scientists* (Wiley-VCH, Weinheim, 2014).

[41] D. Kraft, A software package for sequential quadratic programming, DLR German Aerospace Center Institute for Flight Mechanics Report No. DFVLR-FB 88-28, 1988 (unpublished).